Negative Coulomb Drag in Double Bilayer Graphene

J. I. A. Li,[1] T. Taniguchi,[2] K. Watanabe,[2] J. Hone,[3] A. Levchenko,[4] and C. R. Dean[1]
[1]Department of Physics, Columbia University, New York, New York 10027, USA
[2]National Institute for Materials Science, 1-1 Namiki, Tsukuba, Japan
[3]Department of Mechanical Engineering, Columbia University, New York, New York 10027, USA
[4]Department of Physics, University of Wisconsin–Madison, Madison, Wisconsin 53706, USA
(Received 9 February 2016; published 18 July 2016)

We report on an experimental measurement of Coulomb drag in a double quantum well structure consisting of bilayer-bilayer graphene, separated by few layer hexagonal boron nitride. At low temperatures and intermediate densities, a novel negative drag response with an inverse sign is observed, distinct from the momentum and energy drag mechanisms previously reported in double monolayer graphene. By varying the device aspect ratio, the negative drag component is suppressed and a response consistent with pure momentum drag is recovered. In the momentum drag dominated regime, excellent quantitative agreement with the density and temperature dependence predicted for double bilayer graphene is found.

DOI: 10.1103/PhysRevLett.117.046802

Coulomb drag [1] between parallel quantum wells provides a uniquely sensitive measurement of electron correlations since the drag response depends on interactions only [2–5]. Recently, it has been demonstrated that a new regime of strong interactions can be accessed for devices consisting of two monlolayer graphene (MLG) crystals, separated by few layer hexagonal boron nitride [6–20]. In addition to the unique dispersion of the graphene band structure, advancements in the mechanical assembly of 2D materials make it possible to reduce the interlayer well distance to only a few atomic lengths, while preserving high mobility [21]. Moreover, the ambipolar nature of graphene allows independent control over the carrier type and density in each layer with simple electrostatic gating. In this regime of strong interactions and low disorder, new phases of matter, such as the superfluid exciton condensate, are expected to emerge [22–26].

Drag experiments in double MLG [6–9] have indeed revealed a rich complexity of new behaviors, including a low density response at both zero and finite fields driven by energy coupling mechanisms [18–20], and a high density scaling not captured by existing theories [6]. The precise relationship of these observations to the MLG band structure is the subject of ongoing studies. In a parallel vein, owing to the different single particle energy spectrum and density of states in bilayer graphene (BLG), a significant variation in the drag coefficient is expected for double quantum wells consisting of two BLG layers [10,11]. Moreover, further enhancement of the interaction strength compared to MLG is anticipated, which could, for example, stabilize the condensate phase at higher temperatures [25,26].

Here, we report Coulomb drag measurement in double BLG systems, with interlayer hexagonal boron nitride (hBN) spacers varying from approximately 5 to 12 nm. The double BLG quantum wells are fabricated from exfoliated crystals, using the van der Waals assembly technique described previously in Ref. [21]. In our devices, each BLG is contacted with two pieces of few layer graphite (with a typical thickness of 5–10 nm) serving as electrical leads. The entire heterostructure, consisting of nine layers of exfoliated 2D materials, is assembled on an oxidized, doped Si substrate, then etched into a crossed Hall bar geometry (Fig. 1). The inset in Fig. 1(a) shows a schematic cross section of the full layer structure in the region where the top and bottom layer graphite leads overlap. The carrier density can be tuned independently in the top and bottom BLG layers by biasing the top evaporated metal, and bottom, doped Si gate electrodes, respectively. The graphite leads allow us to tune the BLG layers to the opposite carrier type, while maintaining good electrical contact to each layer (in double BLG, leads defined by etching, such as in previous studies of double MLG structures [6–9] develop a band gap under a transverse magnetic field and become highly resistive). Further details of the device fabrication including the effect of introducing graphite leads can be found in the Supplemental Material (SM) [27].

In a typical drag measurement, the current, I_{drive}, is applied through two corner leads of the drive BLG layer, and the resulting voltage, V_{drag}, is measured from corner leads of the drag BLG layer [Fig. 1(a)]. Figure 1(b) shows an example of the drag resistance, defined by the relation $R_{\mathrm{drag}} = V_{\mathrm{drag}}/I_{\mathrm{drive}}$, plotted as a function of the top and bottom layer densities, n_T and n_B, respectively, acquired at $T = 300$ K. The carrier density of each BLG layer is related to the applied gate voltages by independent measurement of the layer Hall resistivities under an applied magnetic field (see the SM [27]). The density dependence exhibits a four quadrant symmetry, with R_{drag} being negative (positive) when the carriers in the two BLG layers

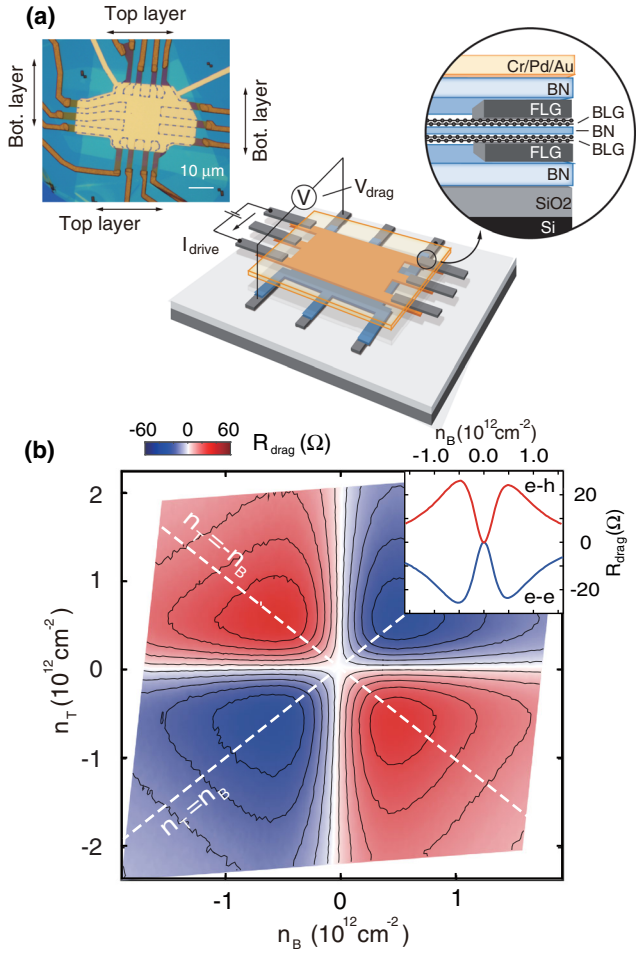

FIG. 1. Coulomb drag. (a) Schematic of a double bilayer graphene device and local Coulomb drag measurement. (Left inset) Optical image of a double bilayer graphene device. (Right inset) Cross section of the bilayer graphene-hBN heterostructure. (b) R_{drag} as a function of n_T and n_B at 300 K from the local drag measurement. The solid curves are isolevels. (Inset) The behavior of R_{drag} at 300 K along match density lines, $n_T = n_B$ (e-e) and $n_T = -n_B$ (e-h).

have the same (the opposite) sign. This is the expected sign relation in a momentum coupling drag picture [18,19], and we adopt the convention of referring to this as positive drag in all four quadrants. We note that all drag responses reported are similar when we switch the drive and drag layers, satisfying the expected Onsager relation.

At $T = 300$ K, the isolevel of R_{drag} suggests a functional dependence of $R_{\mathrm{drag}} = f(n_T + n_B)$, as opposed to the expected form of $f(n_T \times n_B)$ [10,11]. This is consistent with the drag response reported for double MLG [6], suggesting a similar origin for the unconventional, but to date unknown, density dependence. The inset of Fig. 1(b) shows the drag response along the matched density condition, $n_T = \pm n_B$. R_{drag} initially diverges with decreasing density, but it then diminishes to zero near the charge neutrality point (CNP). When the Fermi energy in each BLG layer is tuned to its respective CNP [referred to as

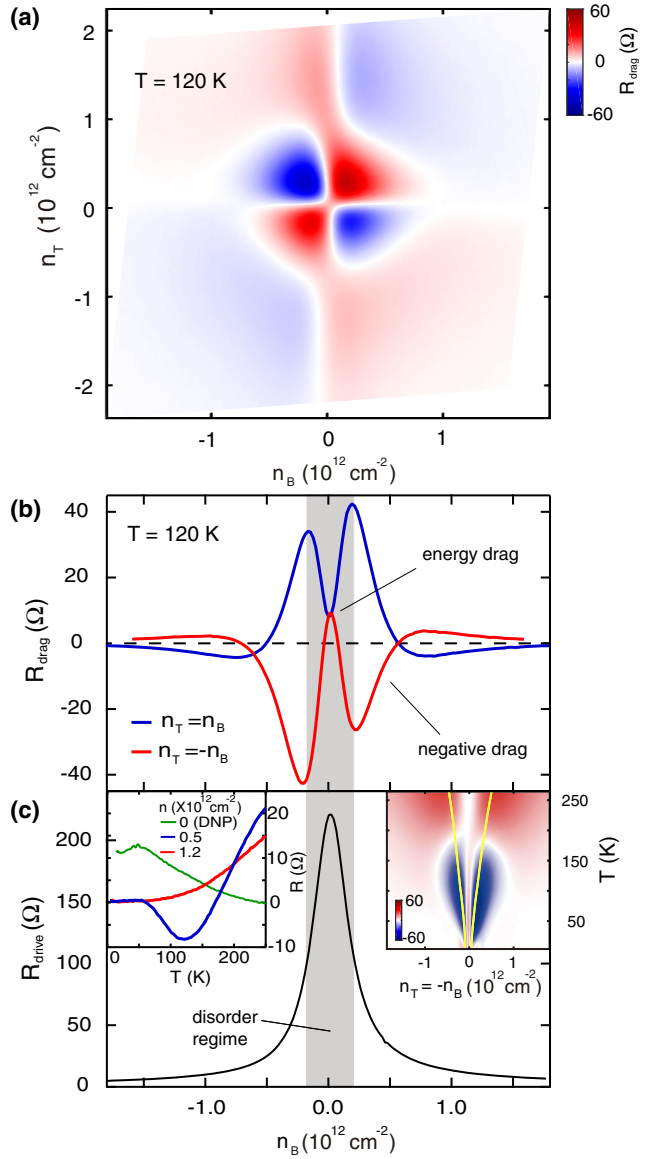

FIG. 2. Negative drag. (a) R_{drag} as a function of top and bottom layer density, n_T and n_B, respectively, at 120 K. (b) R_{drag} along the matched density line, $n_T = \pm n_B$. (c) Drive layer resistivity along the same density line. The approximate charge puddle regime, defined by the full width at half maximum (FWHM) of the resistivity peak, is shown as the grey shaded area. (Left inset) The temperature dependence of R_{drag} at select densities along the $n_T = -n_B$. (Right inset) R_{drag} under the equal density condition, $n_T = -n_B$, at varying temperatures. The yellow solid line marks the FWHM of the drive layer resistivity peak at varying temperatures.

the double neutrality point (DNP)] the drag response drops to zero within our measurement resolution.

Figure 2(a) shows a plot of the drag resistance for the same measurement configuration, but acquired at $T = 120$ K. At this temperature the drag unexpectedly inverts sign in all four quadrants. The inversion regime remains symmetric with R_{drag} positive (negative) when both layers contain carriers with the same (the opposite) sign.

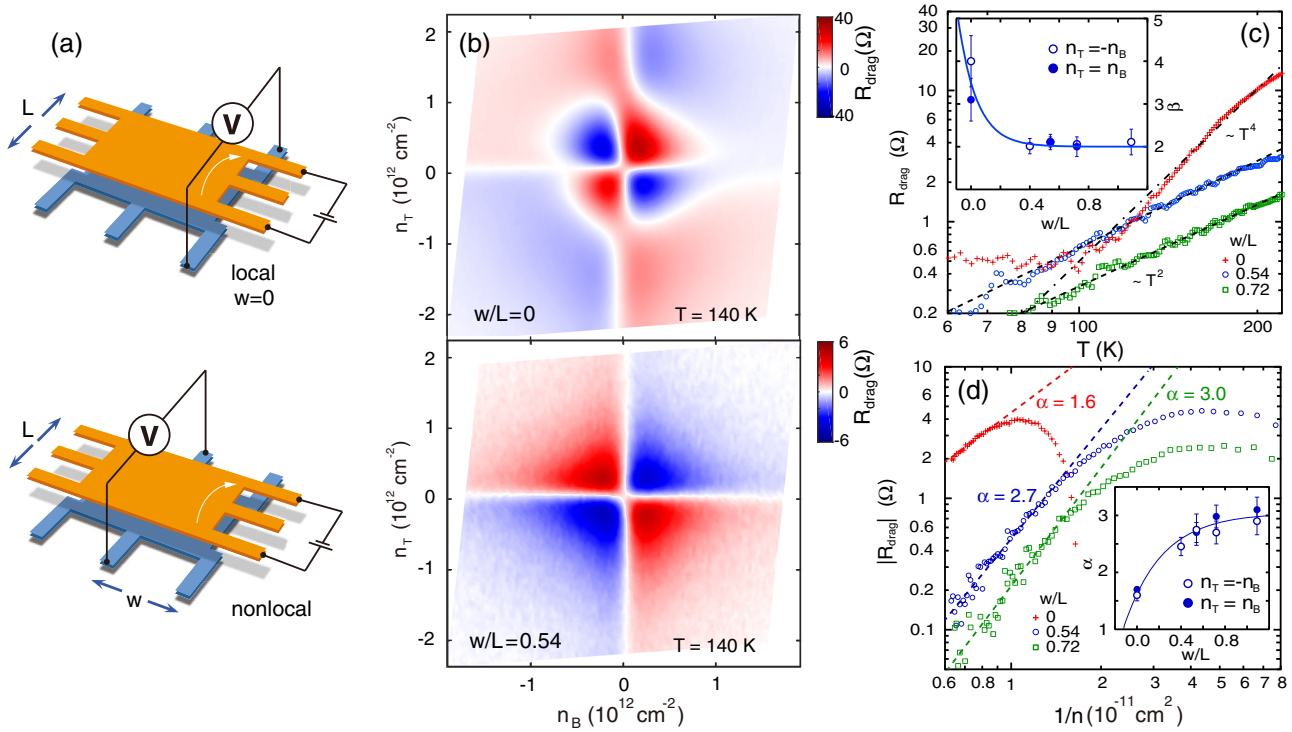

FIG. 3. Local and nonlocal drag. (a) Schematic of the local and nonlocal drag measurement. (b) Density dependence of R_{drag} from a local geometry measured at 140 K (upper panel). Density dependence of R_{drag} from a nonlocal geometry measured at 140 K (lower panel). (c) Temperature dependence of R_{drag} under the equal density condition $n_T = -n_B = 7 \times 10^{11}$ cm^{-2}, taken from local and nonlocal measurements. The black dashed line corresponds to the expected T^2 dependence, and the dash-dotted line is a fit to the local measurement. (Inset) The value of β versus the geometric factor w/L, where β is obtained by fitting R_{drag} with a power law temperature dependence. (d) R_{drag} versus inverse density in the matched density regime, $n_T = n_B$, from the local and nonlocal measurement at $T = 150$ K. The dashed lines are fits to R_{drag} with a power law density dependence. The fit coefficient α is plotted in the inset against the geometric factor w/L.

Examining the response along the matched density lines at low temperature [Figs. 2(b) and 2(c)] reveals three distinct drag regimes. Along $n_T = -n_B$, the sign of the drag is expected to be positive at all densities. Instead, the drag starts out as positive at high density, crosses over to negative at intermediate density, then becomes positive again at near zero density (similar behavior is apparent along $n_B = +n_T$). A full map of the temperature and density dependance is shown in the insets of Fig. 2(c). The high density crossover presumably results from an interplay between the conventional momentum drag and the new negative drag mechanism, suggesting that these two competing contributions have different density dependences. The peak negative drag response coincides approximately with the width of the transport resistivity peak near the CNP, as shown in Fig. 2(c), consistent with a transition to the disorder dominated puddle regime at low density. Importantly, the crossover from positive to negative drag evolves in a nontrivial way and does not track the temperature dependence of the full width at half maximum of the resistive peak near the DNP [see the solid yellow line in the temperature-density plot inset in Fig. 2(c)], suggesting that the onset of the negative drag does not have a simple correlation with the sample disorder. In the density range where negative drag is observed, the maximum displacement field is around 0.07 V/nm, corresponding to an energy gap smaller than 10 meV [28]. The finite drag response at the DNP [the green curve in the Fig. 2(c) inset] shows a similar magnitude and temperature dependence to that observed for the DNP response in double MLG [6], suggests the same energy drag mechanism as the origin of this zero density feature.

Figure 3(b) shows the result of varying the measurement configuration. We characterize the geometry by the ratio w/L, where w is the lateral distance separating the current and voltage leads, and L is the distance between the source and the drain. Schematic illustrations of a "local drag" (defined by $w = 0$) and a "nonlocal drag" ($w \neq 0$) measurement geometry are shown in Fig. 3(a) (we note that, in all measurements, the voltage leads remain parallel to the current leads). In the nonlocal geometry, the negative drag component is suppressed [Fig. 3(b)], and a picture qualitatively similar to the high temperature response is fully recovered. Since interaction is mediated through long-range Coulomb scattering in the momentum transfer picture, we argue that the negative drag originates from a more local interaction between charge carriers.

In the Fermi liquid regime with drag mediated by a momentum-relaxation mechanism, the drag coefficient for double BLG, in the matched density configuration, is expected theoretically to vary with temperature, T, and density, $n = \|n_{T,B}\|$, according to the scaling formula [10,11]

$$R_{\text{drag}} \propto \frac{T^{\beta}}{n^{\alpha}}, \tag{1}$$

with temperature and density power exponents dependent on a particular transport regime defined by the Fermi energy E_F, the Fermi momentum k_F, the interlayer separation d, and the inverse Thomas-Fermi screening radius k_{TF}, respectively. We estimate our samples to be in a strong coupling regime with $k_{TF}d \sim 0.6$, always at temperatures satisfying $T \ll E_F/(k_F d)$ (see the SM [27]), and we therefore expect $R_{\text{drag}} \propto T^2/n^3$.

In Fig. 3(c) we compare the temperature dependence of R_{drag} in the equal density regime $n_T = -n_B$, from the local and nonlocal geometries. In the nonlocal geometry, the response appears to fit a power law well over a large temperature range, whereas the local drag response displays significant deviation. We interpret this to be a consequence of the competing mechanisms of the positive and negative drag components, with the relative contributions apparently varying with temperature. In the inset of Fig. 3(c), the power law coefficient β is plotted against the geometric factor w/L. The contribution from the negative component is increasingly suppressed as the measurement geometry is made more nonlocal, and the power converges to the expected value of $\beta = 2$ within the measurement uncertainty [the same result is observed for $n_T = n_B$ (see the SM [27])]. Figure 3(d) shows the density dependence of R_{drag} in the equal density regime at $T = 150$ K, for different measurement geometries. With increasing nonlocal geometry, the density dependence of R_{drag} converges to the expected $1/n^{\alpha}$ dependance, with $\alpha = 3$ [the inset in Fig. 3(d)]. Both the temperature and the density response suggest that by measuring in the nonlocal geometry we are able to isolate the momentum coupling component of the drag response, and, moreover, we find good quantitative agreement with the theoretically calculated temperature and density dependence for double BLG [10,11].

Finally, we examine the drag response in the presence of a magnetic field. Near the DNP, R_{drag} is shown to be negative in a small magnetic field, and it grows in amplitude with an increasing B field. This behavior is consistent with a previous result from MLG [6], originating from an energy driven Nernst effect [9,18]. At $B = 1$ T, the density dependence of R_{drag} measured at $T = 200$ and 70 K are shown in the lower left and lower right corners of Fig. 4(a). At $T = 200$ K, R_{drag} displays a four quadrant symmetry consistent with momentum drag. At 70 K, R_{drag} changes sign away from the DNP. The sign inversion is particularly clear in the $n_T = n_B$ (e-e and h-h) quadrants, contrasted by the strong negative peak at the DNP.

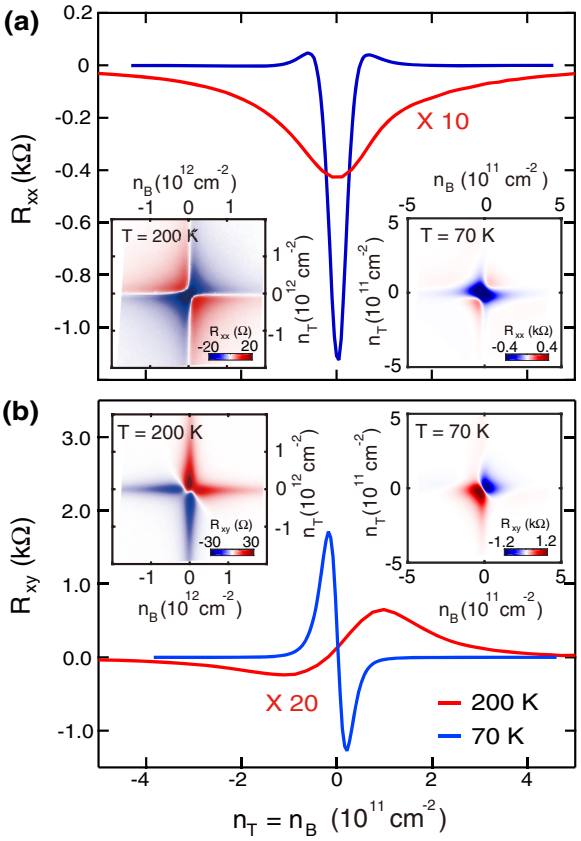

FIG. 4. Magnetodrag. (a) R_{drag} measured at $T = 200$ and 70 K, $B = 1$ T as a function of the match density, and $n_T = n_B$. The density dependence of R_{drag} at (lower left inset) 200 K and (lower right inset) 70 K. (b) Hall drag R_{xy} measured at $T = 200$ and 70 K, $B = 1$ T as a function of match density, and $n_T = n_B$. The density dependence of R_{xy} measured at (lower left inset) $T = 200$ K and (lower right inset) 70 K.

Simultaneous Hall drag measured at 200 and 70 K is shown in Fig. 4(b). Hall drag is expected to be zero in a pure momentum transfer picture and a nonzero Hall drag response has been explained by the field induced coupling between the momentum and energy transfer modes [9,18,20]. In the same temperature regime where we observe negative drag at zero field, we find that the Hall drag response in a finite field also changes sign [Fig. 4(b)]. This behavior is unlike the monotonic response of the Hall drag observed in double monolayer graphene [6].

At present, the origin of the negative drag is not known. Because of its appearance in all four density quadrants, we do not consider this to be related to the formation of indirect excitons between the layers. We find that both the local and nonlocal drag responses appear to be independent of the contact metal and configuration in our devices [29] (see the SM [27]). The suppression in nonlocal geometry suggests that the negative drag results from a shorter relaxation mechanism than can be attributed to a momentum coupling picture. One possibility is that, in the density and temperature range of negative drag, electron liquid is collision

dominated, as a recent measurement in graphene suggests that, at such a temperature, hydrodynamic response plays an important role [30]. Negative drag was also reported for 1D-1D systems [31,32], but there is no obvious reason to believe that there is a relation to the mechanism of negative drag reported here. Similar negative drag behavior at zero field, magnetodrag, and Hall drag responses are observed in all BLG devices studied (with interlayer distances spanning 5–12 nm). We note that negative drag has not been reported for MLG, suggesting a possible relation to the dispersion relation which is quadratic in BLG, compared to linear for MLG.

In summary, Coulomb drag measurement is reported for the first time in a double well consisting of two graphene bilayers. At low temperature and intermediate density, a negative drag is observed with a sign opposite to that expected in a simple momentum coupling regime. We find that the negative drag response can be suppressed using a nonlocal measurement geometry, and that the temperature and density dependence of R_{drag} from nonlocal measurement matches well with the theory for momentum drag [10,11]. In a nonzero magnetic field, Hall drag and magnetodrag observed at high temperatures are consistent with the energy driven mechanism observed in double MLG [9], whereas in the negative drag regime, Hall drag changes the sign. Finally, we note that the negative drag response is fully symmetric and appears for both matched *e*-*e* (*h*-*h*) and mismatched *e*-*h* (*h*-*e*) carrier types. The capability of achieving good electrical contact to a double BLG structure, and to isolate the momentum driven drag component in a nonlocal geometry, over a wide density range makes it feasible to look for the excitonic condensate phase, possibly with smaller interlayer separation and at lower temperatures.

This work was supported by the National Science Foundation (Grant No. DMR-1507788) and by the David and Lucile Packard Foundation. A. L. acknowledges the financial support from NSF Grants No. DMR-1606517 and No. ECCS-1560732, and from the Office of the Vice Chancellor for Research and Graduate Education, with funding from the Wisconsin Alumni Research Foundation.

[1] B. N. Narozhny and A. Levchenko, arXiv:1505.07468.
[2] P. M. Solomon, P. J. Price, D. J. Frank, and D. C. La Tulipe, Phys. Rev. Lett. **63**, 2508 (1989).
[3] T. J. Gramila, J. P. Eisenstein, A. H. MacDonald, L. N. Pfeiffer, and K. W. West, Phys. Rev. Lett. **66**, 1216 (1991).
[4] U. Sivan, P. M. Solomon, and H. Shtrikman, Phys. Rev. Lett. **68**, 1196 (1992).
[5] J. P. Eisenstein, Annu. Rev. Condens. Matter Phys. **5**, 159 (2014).
[6] R. V. Gorbachev, A. K. Geim, M. I. Katsnelson, K. S. Novoselov, T. Tudorovskiy, I. V. Grigorieva, A. H. MacDonald, S. V. Morozov, K. Watanabe, T. Taniguchi, and L. A. Ponomarenko, Nat. Phys. **9**, 775 (2013).
[7] S. Kim, I. Jo, J. Nah, Z. Yao, S. K. Banerjee, and E. Tutuc, Phys. Rev. B **83**, 161401 (2011).
[8] S. Kim and E. Tutuc, Solid State Commun. **152**, 1283 (2012).
[9] M. Titov, R. V. Gorbachev, B. N. Narozhny, T. Tudorovskiy, M. Schütt, P. M. Ostrovsky, I. V. Gornyi, A. D. Mirlin, M. I. Katsnelson, K. S. Novoselov, A. K. Geim, and L. A. Ponomarenko, Phys. Rev. Lett. **111**, 166601 (2013).
[10] E. H. Hwang, R. Sensarma, and S. Das Sarma, Phys. Rev. B **84**, 245441 (2011).
[11] J. Lux and L. Fritz, Phys. Rev. B **87**, 075423 (2013).
[12] M. I. Katsnelson, Phys. Rev. B **84**, 041407 (2011).
[13] N. M. R. Peres, J. M. B. L. dos Santos, and A. H. C. Neto, Europhys. Lett. **95**, 18001 (2011).
[14] B. N. Narozhny, M. Titov, I. V. Gornyi, and P. M. Ostrovsky, Phys. Rev. B **85**, 195421 (2012).
[15] B. Scharf and A. Matos-Abiague, Phys. Rev. B **86**, 115425 (2012).
[16] B. Amorim, J. Schiefele, F. Sols, and F. Guinea, Phys. Rev. B **86**, 125448 (2012).
[17] A. Principi, M. Carrega, R. Asgari, V. Pellegrini, and M. Polini, Phys. Rev. B **86**, 085421 (2012).
[18] J. C. W. Song and L. S. Levitov, Phys. Rev. Lett. **109**, 236602 (2012).
[19] M. Schütt, P. M. Ostrovsky, M. Titov, I. V. Gornyi, B. N. Narozhny, and A. D. Mirlin, Phys. Rev. Lett. **110**, 026601 (2013).
[20] J. C. W. Song and L. S. Levitov, Phys. Rev. Lett. **111**, 126601 (2013).
[21] L. Wang, I. Meric, P. Huang, Q. Gao, Y. Gao, H. Tran, T. Taniguchi, K. Watanabe, L. Campos, D. Muller, J. Guo, P. Kim, J. Hone, K. L. Shepard, and C. R. Dean, Science **342**, 614 (2013).
[22] M. Y. Kharitonov and K. B. Efetov, Phys. Rev. B **78**, 241401 (2008).
[23] H. Min, R. Bistritzer, J.-J. Su, and A. H. MacDonald, Phys. Rev. B **78**, 121401 (2008).
[24] Y. E. Lozovik, S. L. Ogarkov, and A. A. Sokolik, Phys. Rev. B **86**, 045429 (2012).
[25] A. Perali, D. Neilson, and A. R. Hamilton, Phys. Rev. Lett. **110**, 146803 (2013).
[26] M. Zarenia, A. Perali, D. Neilson, and F. M. Peeters, Sci. Rep. **4**, 7319 (2014).
[27] See Supplemental Material at http://link.aps.org/supplemental/10.1103/PhysRevLett.117.046802 for details of sample fabrication and measurement.
[28] Y. Zhang, T.-T. Tang, C. Girit, Z. Hao, M. C. Martin, A. Zettl, M. F. Crommie, Y. R. Shen, and F. Wang, Nature (London) **459**, 820 (2009).
[29] B. Laikhtman and P. M. Solomon, Phys. Rev. B **41**, 9921 (1990).
[30] F. Ghahari, H.-Y. Xie, T. Taniguchi, K. Watanabe, M. S. Foster, and P. Kim, Phys. Rev. Lett. **116**, 136802 (2016).
[31] M. Yamamoto, M. Stopa, Y. Tokura, Y. Hirayama, and S. Tarucha, Science **313**, 204 (2006).
[32] D. Laroche, G. Gervais, M. P. Lilly, and J. L. Reno, Nat. Nanotechnol. **6**, 793 (2011).
[33] J. I. A. Li, T. Taniguchi, K. Watanabe, J. Hone, A. Levchenko, and C. R. Dean, following Letter, Phys. Rev. Lett. **117**, 046803 (2016).